Hindawi
Shock and Vibration
Volume 2022, Article ID 1906498, 13 pages
https://doi.org/10.1155/2022/1906498

Research Article

A Hybrid Model for Predicting Steering Brake Squeal Based on Multibody Dynamics and Finite Element Methods

Lijun Zhang, Yongchao Dong, Dejian Meng, and Wenbo Li

School of Automotive Studies, Tongji University, Shanghai 201804, China

Correspondence should be addressed to Dejian Meng; mdj0218@163.com

Received 21 September 2021; Revised 19 December 2021; Accepted 29 December 2021; Published 12 January 2022

Academic Editor: Selçuk Erkaya

In recent years, the problem of automotive brake squeal during steering braking has attracted attention. Under the conditions of squealing, the loading of sprung mass is transferred, and lateral force is generated on the tire, resulting in stress and deformation of the suspension system. To predict the steering brake squeal propensity and explore its mechanism, we established a hybrid model of multibody dynamics and finite element methods to transfer the displacement values of each suspension connection point between two models. We successfully predicted the occurrence of steering brake squeal using the complex eigenvalue analysis method. Thereafter, we analyzed the interface pressure distribution between the pads and disc, and the results showed that the distribution grew uneven with an increase in the steering wheel angle. In addition, changes in the contact and restraint conditions between the pads and disc are the key mechanisms for steering brake squeal.

1. Introduction

Of various brake friction vibration and noise problems, brake squeal with high frequency (1~16 kHz) and high intensity that often occurs under conditions of low automotive speed and low brake pressure [1] is a friction-induced vibration [2]. The brake squeal that occurs during steer braking is referred to as the steering brake squeal. Compared with the straight-line braking, the steering brake squeal is a new type of brake system noise, vibration, and harshness (NVH) problem, its frequency is low, and its dynamic phenomenon is more unstable. According to the experimental research conducted by Doi et al. [3], during steering braking, the brake disc surface deflects relative to the rotation axis. In bench tests, the test objects are mainly pin-on-disc system [4], cantilever-on-disc system [5], third-body layer [6], brake corner system [7], and chassis corner system [8]. Among them, the brake and suspension system jointly constitute the chassis corner system, which can reproduce low-frequency squeal noise well [9]. The parameters of the chassis corner system include the brake disc [10], lining, caliper, and bracket [11], and noise insulator [12]. If these parameters remain unchanged, there is no squeal during straight-line braking. However, during steer braking, the change in brake restraint conditions may increase the likelihood of squeal.

Inducing unstable vibrations is the most important step in studying brake squeal, according to some researchers; the "stick-slip" theory [13], "variable dynamic friction coefficient velocity" theory [14], "sprag-slip" theory [15], "mode coupling" theory [16], and "unified" theory [17] explain the dynamic phenomena of friction and instability in brake systems. From the perspective of motion dimension, these mechanism models can be classified into one-, two-, and three-dimensional models. The one-dimensional model focuses on the one-dimensional tangential constraint and the contact of the friction pair [18, 19]. A two-dimensional model studies the influence of the contact parameters and structural characteristics on brake squeal [20]. A three-dimensional dynamic model was employed to study the effect of the rich modal frequency of the brake disc on brake squeal [21]. The finite element (FE) modeling of the brake system is an important step in studying brake squeal; Belhocine et al. [22, 23] have rich experience in FE modeling, especially the selection for element type and meshing, which provides a significant reference value for this study. Under the

conditions of braking, heat is generated between the pads and disc owing to friction, and it directly affects the contact characteristics of the brake system [24, 25]. Herein, we study the squeal characteristics under conditions of straight line and steering braking. The temperature of the brake disc was controlled during the process of the vehicle road test.

In terms of numerical simulation analysis, mainstream brake squeal simulation approaches include the complex eigenvalue analysis (CEA) method [26] and the transient dynamics analysis method [27]. Owing to the high computational cost of temporal methods, transient dynamics analysis is used in simple systems, such as pads-on-disc system [28] and brake corner system [29]. The frictional force is introduced by the CEA method into the friction pair such that the stiffness matrix becomes asymmetric and generates complex eigenvalues, which can be used to predict brake squeal propensity, and is widely used in automotive brake squeal research. Stump et al. [30] showed that the restraint conditions of the pad and caliper are different, which is the reason for the brake squeal under forward and backward conditions. Therefore, in the process of FE modeling, we should focus on the physical parameters of the chassis corner restraint conditions.

Previous studies focused on squeal during straight-line braking, and they ignored the contact state changes between the pads and disc caused by the change in wheel angles and the deformation of the suspension system during steering operations. The six-dimensional wheel forces and wheel angles during straight and steer braking vary significantly; therefore, the suspension systems are affected by different forces. The main purpose of this study is to establish a hybrid model of multibody dynamics (MBD) and FE, predict the brake squeal propensity during automotive turning operations, and explore basic mechanism based on the above-mentioned analysis. Thus, this study provides an effective reference for the design and engineering applications of brake systems.

2. Model Analysis during Steer Braking

2.1. Complex Eigenvalue Analysis. The coupling between the pads and disc is equivalent to providing a disturbance loading on the brake system, and the free vibration equation of motion for the brake system is as follows:

$$[M]\left\{\ddot{X}\right\} + [C]\left\{\dot{X}\right\} + [K]\{X\} = \{0\}, \tag{1}$$

where $[M]$, $[C]$, $[K]$, and $\{X\}$ are the mass matrix, damping matrix, stiffness matrix, and displacement of the discrete nodes, respectively. During the braking, the force applied by the piston acts perpendicularly on the pad and generates frictional force between the pads and disc to achieve deceleration. If the effect of friction is included, the vibration equation is as follows:

$$[M]\left\{\ddot{X}\right\} + [C]\left\{\dot{X}\right\} + \left[K - K_f\right]\{X\} = \{0\}, \tag{2}$$

where K_f is the friction stiffness matrix. The existence of frictional force can cause asymmetry in the system stiffness matrix $[k]$ and excite the unstable modes of the system. By solving complex eigenvalues, including the real and imaginary parts, the brake squeal propensity can be predicted. The positive real part can expand the vibration and develop into a strong self-excited vibration, resulting in the instability of the system. Therefore, the real part of the eigenvalue is an important indicator for determining whether a brake squeal will occur.

2.2. Effect of Roll Motion on LTR. The driver's steering input causes the vehicle to roll, and current research on roll estimation is based on the lateral dynamics model. The classical two-degrees-of-freedom model ignores the effect of suspension; the longitudinal speed is assumed to be constant; only the yaw and lateral motions are considered, as shown in Figure 1(a). Based on the above model, a lateral dynamic model with three degrees of freedom, as shown in Figure 1(b), was established by adding a degree of freedom of roll motion. It is defined as rollover when the inner tire is off the ground because the left and right tires are transferred under the action of lateral vehicle force; therefore, the load transfer ratio (LTR) is used as the rollover index between the left and right sides of the vehicle [31]. The LTR can be expressed as follows:

$$\mathrm{LTR} = \frac{F_{r,w} - F_{l,w}}{F_{r,w} + F_{l,w}}, \tag{3}$$

where $F_{r,w}$ and $F_{l,w}$ are the right and left vertical tire forces, respectively. The value of LTR ranges from −1 to 1. Under the conditions of straight-line braking, $F_{r,w}$ equals $F_{l,w}$, and the value of LTR equals 0. Therefore, the value of LTR represents the degree of load transfer of the sprung mass.

Considering that the roll angle of the unsprung mass is smaller than that of the sprung mass, to simplify the analysis, the roll motion of the unsprung mass is ignored and a more general LTR expression is proposed. Here, a_{m2} represents the lateral acceleration of the sprung mass; the sprung mass rolls around the roll axis R, and the roll angle is ϕ. The vertical loads on the left and right sides of the vehicle are transferred under the combined action of the lateral force and gravity. Assuming that the height of the center of gravity of the unsprung mass is h_1, according to the principle of moment balance,

$$\left(F_{r,w} - F_{l,w}\right)\frac{d}{2} = m_1 a_y h_1 + m_2 a_{m2}\left(h\cos\phi + h_{rc}\right) + m_2 g h \sin\phi. \tag{4}$$

Because the roll angle is relatively small, $\sin\phi \approx \phi$, $\cos\phi \approx 1$; it can be shown that the rollover index can be approximately represented as follows [31, 32]:

$$\mathrm{LTR} = \frac{\left[2\left(m_1 h_1 + m_2\left(h + h_{rc}\right)\right)a_{m2} + m_2 g h\phi + m_1 h_1 h\ddot{\phi}\right]}{mgd}, \tag{5}$$

where m, m_1, and m_2 are the entire vehicle mass, unsprung mass, and sprung mass, respectively; h, h_1, and h_{rc} are the roll radius, centroid height of the unsprung mass, and ground clearance of the roll center, respectively; and d is the

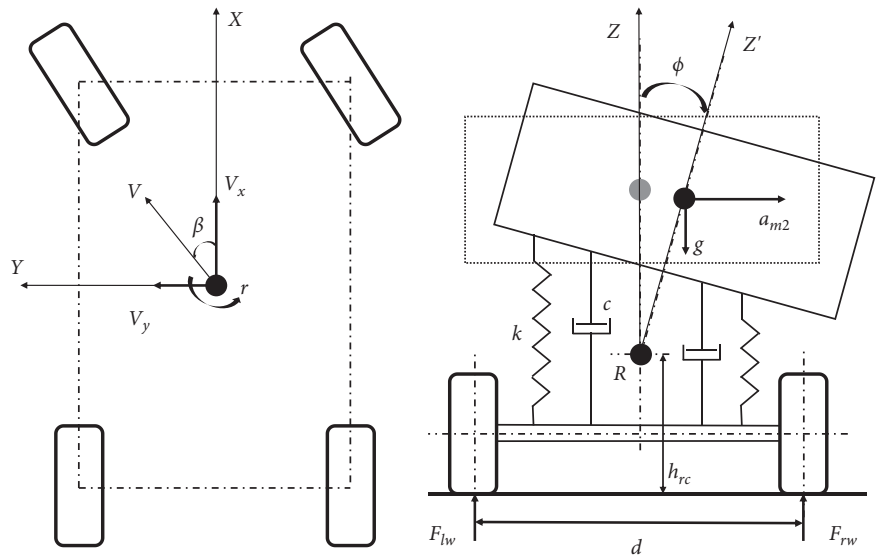

Figure 1: Modeling for vehicle lateral dynamics. (a) Model of two degrees of freedom. (b) Model of three degrees of freedom.

track of the vehicle. The value of LTR is related to the vehicle parameters and is affected by the vehicle movement state. When the vehicle parameters are fixed, the lateral acceleration of the sprung mass, a_{m2}, roll angle, ϕ, and the roll angle acceleration, $\ddot{\phi}$, directly affect the value of LTR; larger lateral acceleration, a_{m2}, and softer suspension will cause a larger value of LTR. At the same vehicle longitudinal speed, the roll angle, ϕ, increases with the increase in steering angle during steering braking, resulting in a significant sprung mass load transfer. Simultaneously, a greater tire lateral force is generated owing to steering; the load transfer from the sprung mass to the unsprung mass and the tire lateral force can inevitably lead to a different stress state of the left and right suspension systems, which can change the contact and restraint conditions between the pads and disc, and aggravate the asymmetry of the stiffness matrix $[K]$ and damping matrix $[C]$ of the system; thus, there is a brake squeal that is more likely to occur during steer braking.

2.3. Multibody Dynamics of Rigid-Flexible Coupling Model. The components of the suspension system are abstracted as rigid or flexible bodies, and they are connected and constrained by each other to form a multibody system. To deform the suspension system, we need to make the suspension components flexible. For a rigid body, six generalized coordinates, such as the Cartesian coordinates of its center of mass in the inertial reference system, and the Euler angle reflecting the orientation of the rigid body are selected, and the dynamic equation is obtained using the Lagrange multiplier method as follows:

$$\frac{\mathrm{d}}{\mathrm{d}t}\left(\frac{\partial T}{\partial \dot{q}}\right)^T - \left(\frac{\partial T}{\partial q}\right)^T + \varphi_q^T p + \theta_q^T \mu - Q = 0, \tag{6}$$

where T is the energy of the system, q is the generalized coordinate column vector, Q is the generalized force vector, p is the Laplace multiplier vector of complete constraints, and μ is the Laplace multiplier vector of noncomplete constraints. The dynamic equation of a single flexible body is as follows:

$$M_f\ddot{\xi} + \dot{M}_f\dot{\xi} - \frac{1}{2}\left(\frac{\partial M_f}{\partial \xi}\dot{\xi}\right)^T\dot{\xi} + K_f\xi + f_g + D_f\dot{\xi} + \left(\frac{\partial \Omega}{\partial \xi}\right)^T\lambda = Q, \tag{7}$$

where M_f and $\dot{M}_f$ are the mass matrix of the flexible body and its first derivative, respectively; ξ, $\dot{\xi}$, and $\ddot{\xi}$ are the generalized coordinate and its first and second derivatives, respectively; K_f and D_f are the stiffness matrix and damping matrix, respectively; f_g is the gravity; Ω is the constraint equation; and λ is the Lagrange multiplier. The equations formed by the above formula are the dynamic equations of the rigid-flexible coupling system of the front suspension, and the dynamic results in the movement process can be obtained using the MBD simulation software.

3. Modeling Process of the Hybrid Model

3.1. Overall Modeling Process. In this study, we propose a method for predicting brake squeal propensity based on the MBD and FE methods, establish a flow chart as shown in Figure 2, and describe the acquisition of key parameters and the detailed modeling process of their relationship. *Stage 1*. A vehicle road test was designed to reproduce brake squeal and to obtain the values of brake pressure, sound pressure, and six-dimensional wheel force when squeal occurs. *Stage 2*. We established a hybrid model, including the rigid-flexible coupling model of the front suspension MBD based on ADAMS and the finite element model (FEM) of the chassis corner based on ABAQUS, where the point is the transfer of the displacement values of each suspension connection point between the MBD model and FEM. The CEA results are also compared to the experimental values. *Stage 3*. The interface

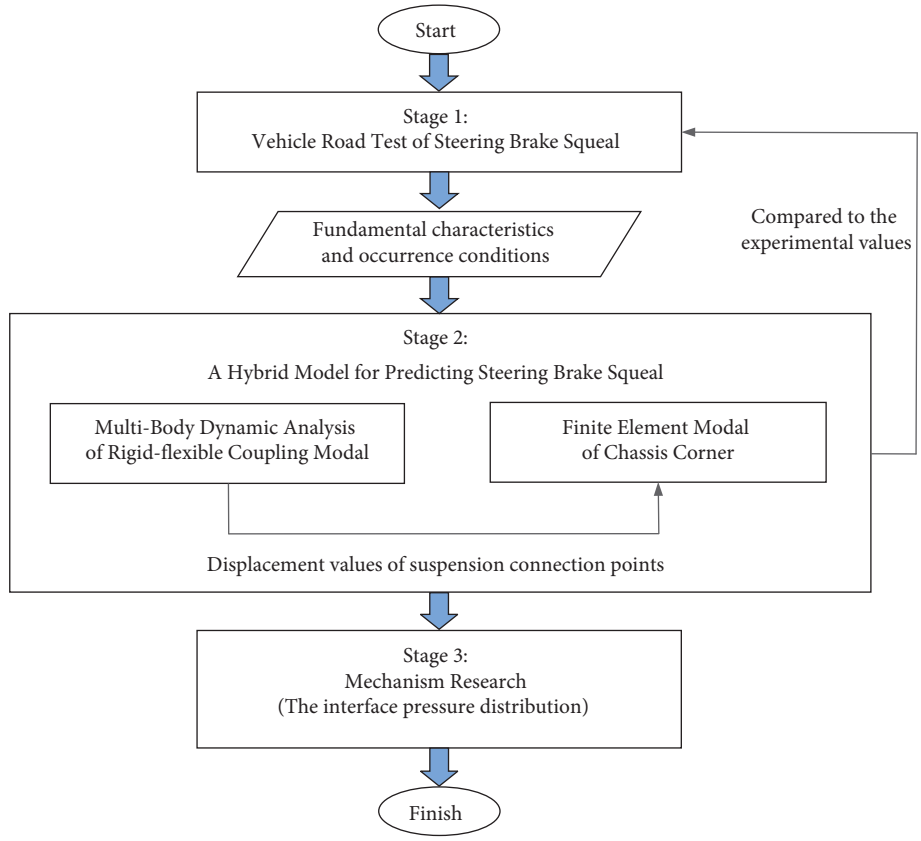

Figure 2: Three stages in the analysis of steering brake squeal propensity.

pressure distribution between the pads and disc under different steering angles was analyzed for exploring the steering brake squeal mechanism.

3.2. Fundamental Characteristics and Occurrence Conditions of Steering Brake Squealing. For the differences between straight line and steering braking, we conducted a vehicle road test to measure the fundamental characteristics of the steering brake squeal; the test object was a compact vehicle equipped with an EHPS system, the power steering fluid was sufficient, and a variety of sensors were installed to measure the fundamental characteristics of the steering brake squeal, as shown in Figure 3. The braking action can be summarized as follows: first, the pressure generated by braking is applied to the piston, and the caliper is pushed by the reaction force; the inner friction pad is then pushed by the piston until it contacts the brake disc, and the outer friction pad is pushed by the caliper against the opposite side of the disc; thus, frictional force is generated between the pads and disc. When the driver implements a braking procedure, the vehicle sometimes deviates from the original driving route to one side of the road. This is the phenomenon of automobile braking deviation, and it is difficult for a driver to safely maintain the desired path by constantly applying steering wheel corrections. However, in this study, the initial braking

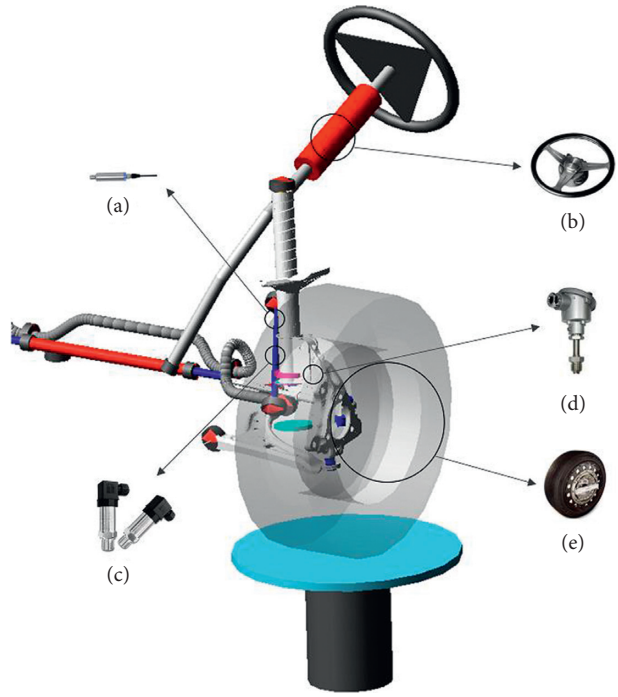

Figure 3: Schematic of sensor arrangement. (a) Sound pressure sensor. (b) Steering angle sensor. (c) Oil pressure sensor. (d) Temperature sensor. (e) Six-dimensional wheel force sensor.

speed was set low, and the road adhesion coefficient was set high; thus, the phenomenon of braking deviation was not considered. According to the standard of brake squeal test [9], a vehicle road test condition is set as follows: the brake oil pressure is set at approximately 1.0 MPa, the initial speed is 10 km/h, and the steering wheel angles are set at straight (0°), turn right ¼ turn (90°), ½ turn (180°), ¾ turn (270°), 1 turn (360°), and $^5/_4$ turn (450°), respectively. While steering, a low-power steering fluid can lead to heavy steering and even abnormal noise and affects the normal operation of the steering system. Brake squeal because of the modal coupling between the pads and disc, and the power steering fluid does not influence brake squeal. Moreover, owing to sliding by the brake pads and fluctuating loads caused by the braking load, heat is generated on the pads and disc [33], and with the increase in vehicle mileage, a small amount of wear occurs on brake pads [34]; it is widely believed that brake pad wear and thermal load can affect brake squeal characteristics. Before the test, the initial temperature of the brake disc must be measured by the temperature sensor, which is ambient temperature, and after each operation of braking, the brake disc needs to be cooled, such that the temperature is controlled near the initial temperature. In the entire life cycle of the vehicle, the wear of the brake pad is particularly important: the wear rate of the pad per 5000 km is approximately 1.316 mm [35]. When the brake pads are relatively new, the number of braking instances is less, and the time is short; therefore, brake pad wear can also be ignored.

Figure 4 shows the characteristics of steering brake squeal, including the time-frequency domain analysis that lasted 1.2 s and the frequency-sound pressure of squeal generated. It can be observed that under the condition of turning right for $^5/_4$ turns, the maximum noise sound pressure can reach 80 dB and the frequency with highest energy is 3289 Hz. In contrast, the energy of other frequency components becomes much smaller, most of which appears with the peak value in the lower frequency band within 2700 Hz, and the sound pressure is less than 65 dB, which is caused by engine and road noises. The working condition of turning right for $^5/_4$ turns can be regarded as the condition under which steering brake squeal.

When the vehicle is moving on the road, three-axis forces and three-axis torques are applied to the wheel, as shown in Figure 5. We analyzed its noise characteristics for the condition of turning right for $^5/_4$ turn braking. The results show that the steering brake squeal primarily occurs in the second half of braking, the wheel speed decreases from approximately 20 r/min to 0 r/min, and the brake pressure and wheel angle are relatively stable when the squeal occurs. The brake pressure is approximately 1.0 MPa, and the steering wheel angle is approximately 480°.

Owing to the influence of road roughness, the vehicle speed changes, and the manual control of the brake pedal. The six-dimensional wheel force fluctuates significantly; however, the change in the six-dimensional wheel force is relatively stable during the occurrence of the squeal. We selected the relatively stable 0.8 s domain curve of the front wheel six-dimensional wheel force for analysis, as listed in Table 1. It shows that the values are relatively stable and can be treated as a constant. In the next section, the real brake oil pressure, steering wheel angle, and six-dimensional wheel force during steer braking are input into the MBD model.

3.3. Modeling and Verification of the MBD Model. MBD model based on ADAMS is an important means of analyzing the dynamic performance of a suspension assembly. To obtain the force and deformation of the suspension assembly under conditions of squeal occurrence, the MBD model of the front suspension, including the McPherson suspension system, stabilizer bar system, and rack and pinion steering system, is established. According to the actual assembly relationship of the front suspension component, the topological relationship can be simplified, as shown in Figure 6. Note that the spindle head and the knuckle are connected through the hub bearing, but in developing the analytical modeling, it is a revolute joint connection.

To deform the suspension assembly, we refer to the modeling method of establishing the suspension multibody dynamic model for braking groan [36] and make flexible lower control arm, steering tie rad, knuckle, and strut. The final rigid-flexible coupling model of the front suspension MBD is shown in Figure 7(a).

A suspension K&C test, including static and dynamic tests, was conducted to verify the accuracy of the MBD model. The K&C static characteristics test of the front suspension involves fixing the vehicle body, applying displacements, forces, or steering wheel angles at the tire contact mark, and measuring the kinematic and elastokinematic characteristics of the suspension. In the dynamic test, the six-dimensional wheel forces and the steering wheel angles measured under the conditions of squeal occurrence were used as inputs, and the strain was obtained by pasting strain gauges on the steering knuckle and suspension components. Simultaneously, the numerical simulation analysis of the same working condition was conducted in ADAMS to compare with the experimental values to verify whether the multibody dynamics model we established is correct.

3.4. Displacement Values of Suspension Connection Points. In the vehicle road test, we found that the working condition for turning the steering wheel right for $^5/_4$ turns is a trigger for brake squeal, and that it is necessary to put the experimental values into ADAMS. We selected the more stable six-dimensional wheel forces, as listed in Table 1, loaded them to the center of the left and right wheels, turned the steering wheel by 480°, and conducted the front suspension MBD simulation. The suspension in the model can deform because of its flexible characteristics, and the deformation is concentrated at the connection between the knuckle and steering tie rod, knuckle and the lower control arm, and the middle of the steering tie rod. For the convenience of analysis, we selected the connection points of the suspension as the loading points. Figure 7(c) shows an example of a lower control arm with a total of three loading points. Lca_front and LCA_rear are the points of the lower control

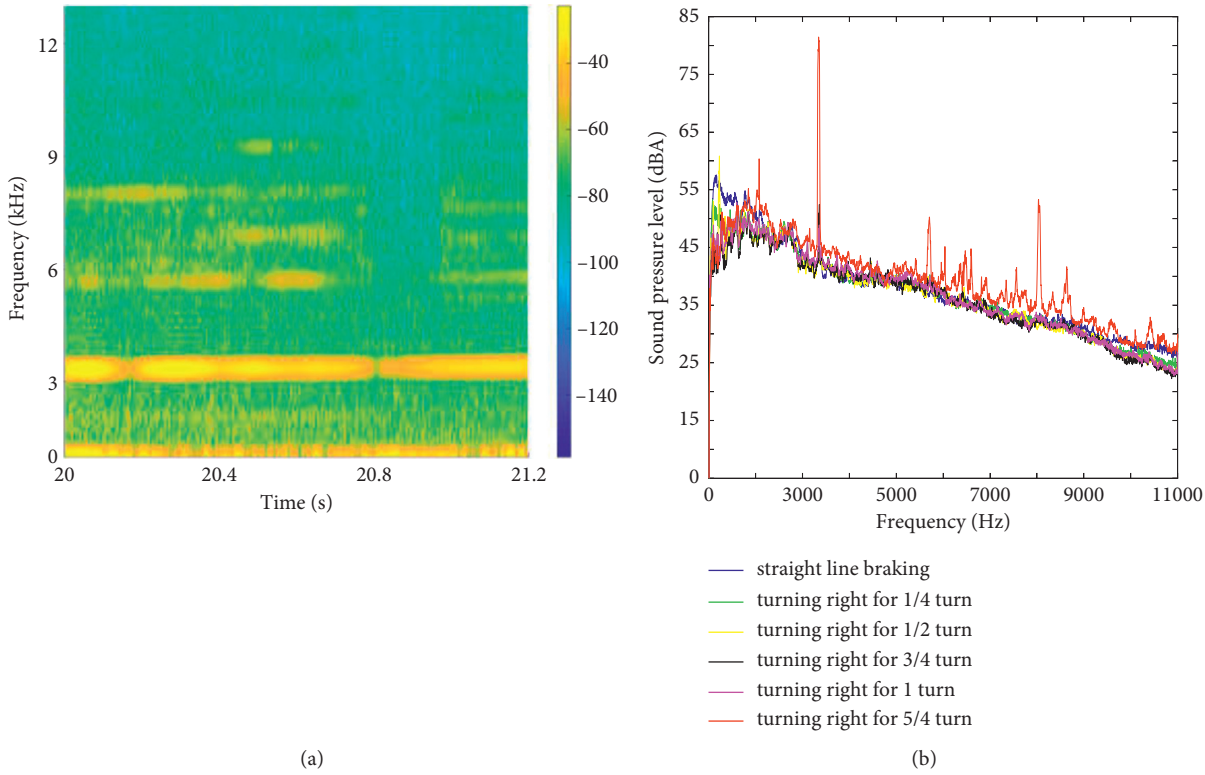

Figure 4: Characteristics of steering brake squeal. (a) Analysis of time domain. (b) Analysis of frequency domain.

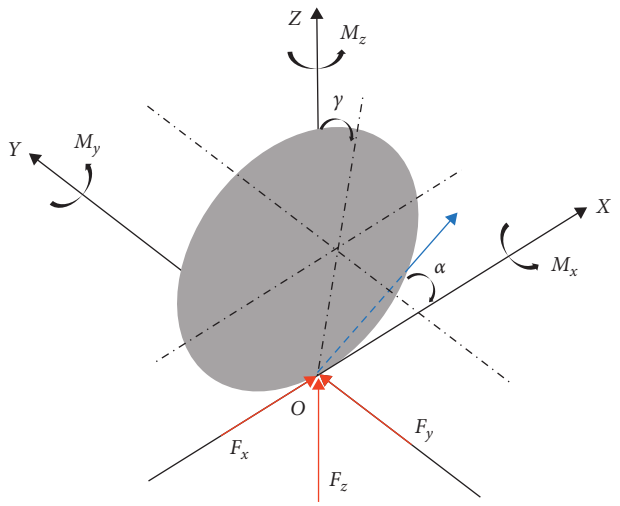

Figure 5: Schematic of six-dimensional wheel force. F_x: longitudinal force, F_y: lateral force, F_z: vertical force, M_x: heeling moment, M_y: twist torque, M_z: aligning torque, α: sideslip angle, and γ: camber angle.

arm and the subframe connected by the bush, and LCA_out is the point where the lower control arm and knuckle are connected through the hinge.

In the FEM, the displacement values of the connection points can completely transfer the force and deformation characteristics; therefore, it is necessary to extract the deformation values of the MBD model. As a result, it was found that steering brake squeal occurs when the wheel speed decreases from 20 to 0 r/min, while the FE analysis only needs to place the displacement at a certain moment as the boundary condition. Here, we select the displacement values at the instant when the wheel speed is 10 r/min. The three-direction linear and angular displacements of the flexible body connection points are presented in Table 2.

3.5. Modeling Process of the Finite Element Model of Chassis Corner. The FEM of the chassis corner is consistent with the front-left chassis components of the road test vehicle. The knuckle, steering tie rod, lower control arm, and strut should be consistent with those of the MBD model, especially for the FEM mesh generation, and to accurately transfer displacement values between the MBD model and FEM, it is necessary to maintain the mesh information of the suspension components consistent. The mesh information is presented in Table 3.

The lower control arm, steering tie rod, and strut are connected to the ground through a bushing, hinge, and spring. The stiffness settings of the front and rear bushings of the lower control arm are consistent with those of the MBD model, which is a nonlinear stiffness. The vertical stiffness between the strut and the ground in the vehicle coordinate system is consistent with that of the actual strut.

The final established FEM of the chassis corner is shown in Figure 8(a). The load includes braking pressure applied to the caliper and piston and rotating speed to the disc. The braking pressure is 1 MPa and the rotating speed is 1.05 rad/s, which is consistent with the condition when brake squeal occurs in the road test. As mentioned above,

Table 1: Values of six-dimensional wheel force during steer braking under condition of squeal occurrence.

Suspension system	F_x (kN)	F_y (kN)	F_z (kN)	M_x (kN·m)	M_y (kN·m)	M_z (kN·m)
Left suspension	−1.01 ± 0.04	0.85 ± 0.02	4.04 ± 0.11	0.87 ± 0.03	−0.02 ± 0.01	0.27 ± 0.03
Right suspension	−1.02 ± 0.03	−0.64 ± 0.02	3.96 ± 0.05	−0.81 ± 0.02	−0.01 ± 0.01	0.19 ± 0.01

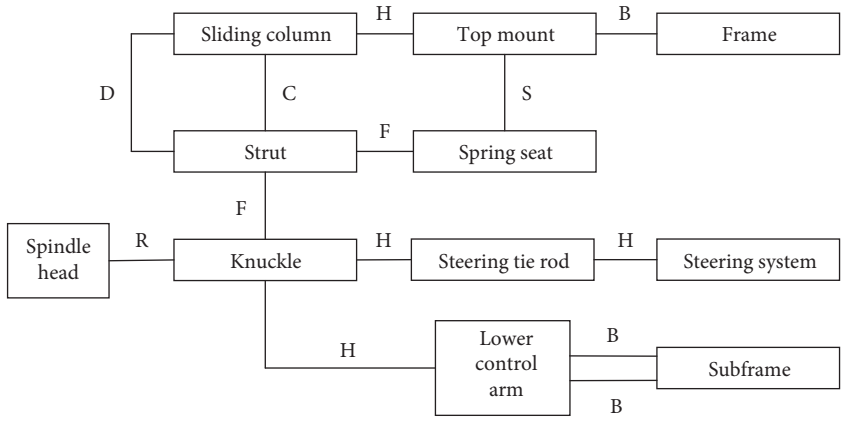

Figure 6: Topological relationship of front suspension assembly. B: bushing, H: hinge, S: spring, D: damping, R: revolute joint, F: fixed joint, and C: column joint.

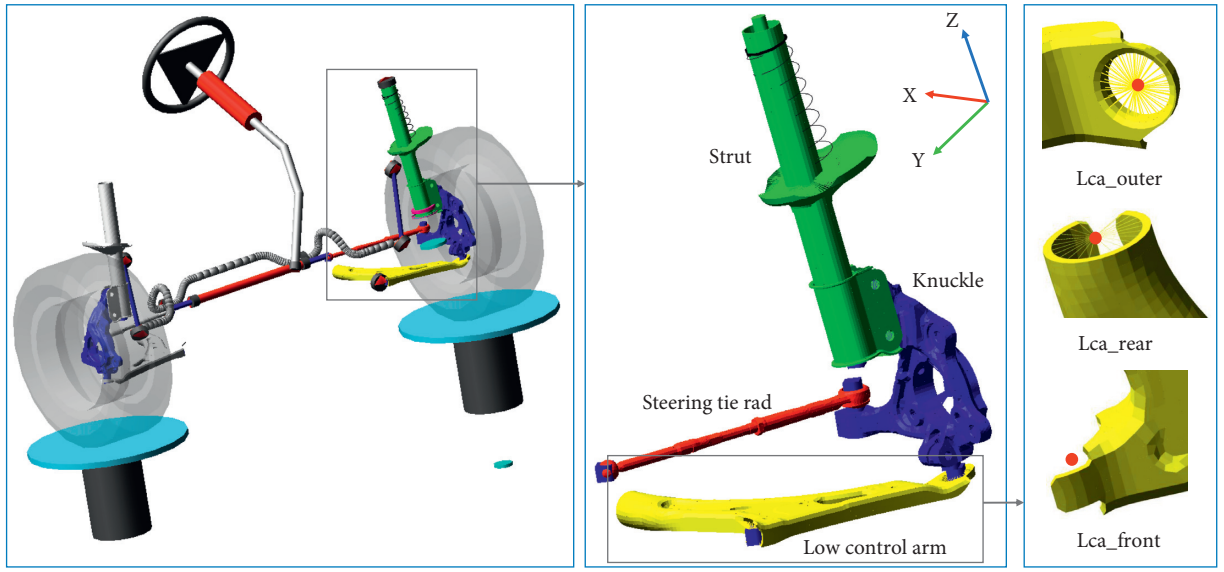

Figure 7: Rigid-flexible coupling model of front suspension assembly. (a) Front suspension assembly. (b) Chassis corner assembly. (c) Low control arm.

Table 2: Partial displacement values of suspension components connection points.

	Lca_front	Lca_outer	Lca_rear	Strut_spring	Strut_dampling	Strut_knuckle
X (mm)	−2.3982	−6.7473	−2.2725	13.0352	26.2526	2.8734
Y (mm)	−0.7266	−0.6561	−3.4505	−3.5987	−7.7315	−2.1511
Z (mm)	0.061	6.1145	−0.3311	4.8305	4.447	5.4883
Rx (rad)	−0.01756	−0.01817	−0.01832	−0.0429	−0.0429	−0.0429
Ry (rad)	−0.00011	−0.00371	0.000306	−0.09563	−0.09563	−0.09563
Rz (rad)	−0.01337	−0.01574	−0.01043	−0.4563	−0.4563	−0.4563

Table 3: Mesh information of suspension components.

Parts	Size (mm)	Type and number of elements						Number of nodes
		C3D6	C3D8I	C3D10	S3	S4R	Numbers	
Lower control arm	4	44	2096	—	—	—	2140	4562
Steering tie rod	4	—	—	7826	—	—	7826	14767
Strut	5	—	4505	—	148	1840	6493	11471
Knuckle	4	—	—	32936	—	—	32936	55355

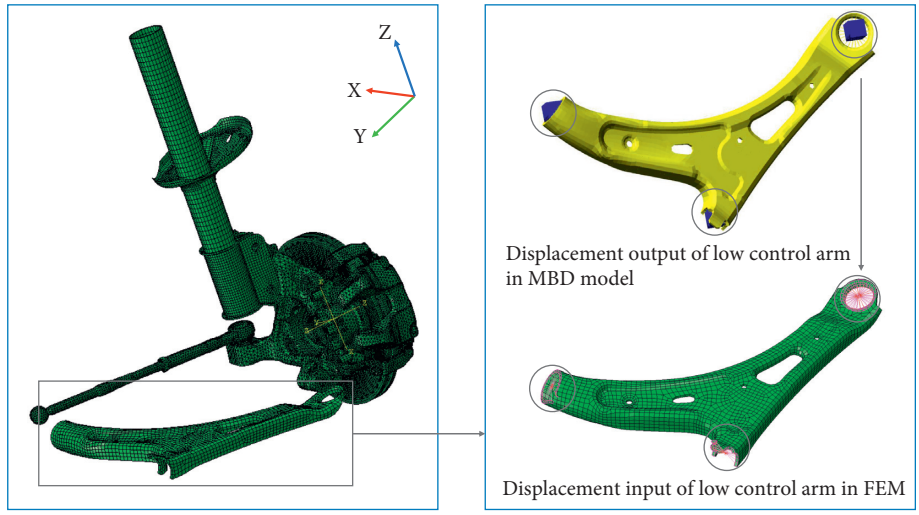

Figure 8: FEM of chassis corner. (a) Chassis corner assembly. (b) Example of values transmission.

the major challenge is to put the displacement values of the flexible body connection points (as shown in Table 2) from the MBD model in the previous step into the corresponding loading points of the FEM, using the low control arm, as shown in Figure 8(b), in which the FEM surface is coupled to the center point, and the displacement values obtained are applied to the coupling point.

4. Results

4.1. K&C Test Verification of the MBD Model. The K&C characteristic test of the front suspension was conducted in Section 3.3, and the test results were compared to numerical results to validate the accuracy of the MBD model; some of the results are shown in Table 4. It was found that the correlation with the tested values was good, with uncertainty under 10%. We can safely conclude that the rigid-flexible coupling model of the front suspension MBD is accurate and effective.

4.2. Complex Eigenvalue Analysis of Finite Elements. Brake squeal is believed to be caused mainly by friction-induced dynamic instability, and thus, the friction coefficients affect the stability of the system. Here, the friction coefficient varying from 0.2 to 0.45 is studied. After setting the corresponding parameters, we conducted the CEA, and the results of the complex modal analysis output the eigenvalues and modal shapes of the system. In the vehicle road test, as shown in Figure 4, the frequency of squeal with high energy is 3289 Hz, where we consider the range where the frequency of squeal frequency fluctuates about 100 Hz as the simulation frequency band. As listed in Table 5, the unstable frequencies in the frequency band appear under different friction coefficients, and the frequencies decrease with the increase in friction coefficients; the real part first increases and then decreases. The results are close to the measured value, with differences dropping below 2%.

The unstable complex modes obtained with different friction coefficients in the simulation frequency band were all 67th-order complex modes, and the mode shapes were consistent, as shown in Figure 9. Here, we consider the simulation result with a friction coefficient $\mu = 0.4$ for analysis; the mode shape corresponding to 3346 Hz is mainly the deformation of the brake system, including disc, pads, and bracket, the deformation of the bracket is the largest, and the deformation of the disc is close to the (0, 3) vibration mode [37]. The inner pad was mainly deformed in the left part and two ears, and the outer pad was mainly deformed in the lower left part and left ear.

The modal assurance criterion (MAC) was used to compare the response variables of the complex mode and vehicle road test. The MAC represents the degree of correlation between a pair of vectors [38], which can be a complex mode vector, real mode vector, or response vector under external excitation and is expressed as follows:

Table 4: K&C characteristics of suspension-comparison of the experimental and numerical analysis results.

Parameters	Roll stiffness (Nm/deg)	Steering angle transmission ratio		Vertical stiffness of wheel center (N/mm)	
		Left wheel	Right wheel	Left wheel	Right wheel
Values of test	1221.62	0.06	0.06	77.2	72.5
Values of simulation	1127.3	0.06	0.06	76	74.1
Margin of error (%)	7.7	−3	−3	−1.5	2.3

Table 5: Complex eigenvalue for different friction coefficients.

Friction coefficient (μ)	0.2	0.25	0.3	0.35	0.4	0.45
Real parts	87.18	95.46	107.28	118.83	106.88	84.75
Frequencies (Hz)	3352	3351	3349	3347	3346	3336

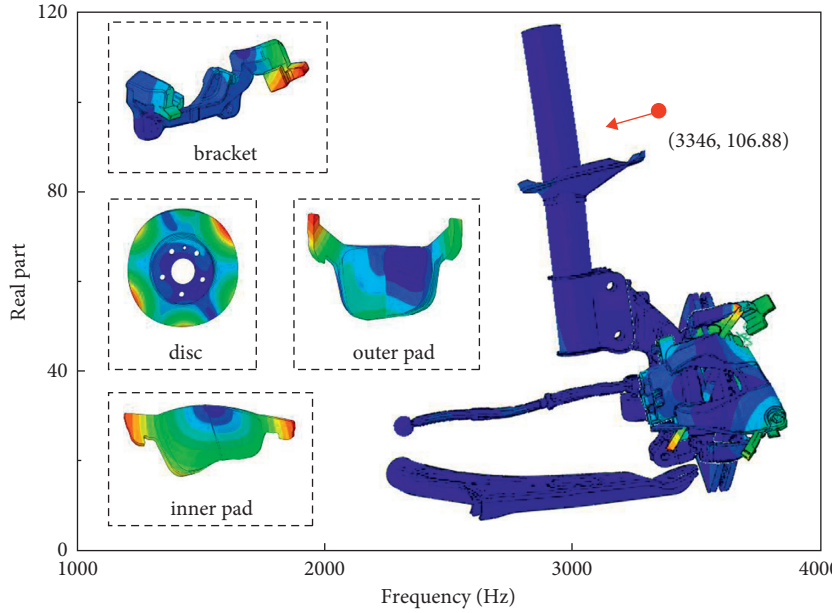

Figure 9: CEA results of chassis corner.

$$\mathrm{MAC}(a,b) = \frac{\left|\sum_{k=1}^{N} a_k b_k^*\right|^2}{\sum_{k=1}^{N} a_k a_k^* \sum_{k=1}^{N} b_k b_k^*}, \tag{8}$$

where a_k and b_k are the vector of the complex mode and the response, $\mathrm{MAC}(a,b)$ is the correlation degree between the ath and bth modes, and its value ranges from 0 to 1, which contains the amplitude and phase information. From the comparison results, the MAC matching degree of the numerical analysis and vehicle road test was 76%. From the two aspects of squeal frequency and MAC, the established hybrid model of MBD and FE can accurately predict the steering brake squeal phenomenon.

5. Mechanism Research

5.1. Numerical Simulation Analysis Results for Different Steering Wheel Angles. The load transfer from the sprung mass to the unsprung mass and the tire lateral force leads to different stress states of the left and right suspension systems, resulting in a change in the interface pressure distribution between the pads and disc. In addition to the frictional force and pressure applied to the pads by the brake disc, the inner and outer pads are also subjected to the axial surface pressure from the piston and caliper finger, and the action areas, positions, and local surface pressures on the pads are different; therefore, the distribution of contact pressure on the two brake pads should be analyzed. As shown in Figure 10, for the outer friction pad, the friction contact area evenly covers the upper half during straight braking. However, with the increase in the steering wheel angle, the distribution of the friction area gradually moves from the upper left part to the right and finally concentrates on the upper right corner. For the inner pad, the friction contact area was evenly distributed in the upper middle. With the increase in the steering wheel angle, the friction area gradually moved downward and finally concentrated in the lower middle part. The average contact pressure between the pads and disc also showed an increasing trend with an increase in the steering wheel angle.

To quantitatively analyze the distribution of the contact pressure, the root mean square deviation, S_q, and an evaluation index describing the surface topography of the brake

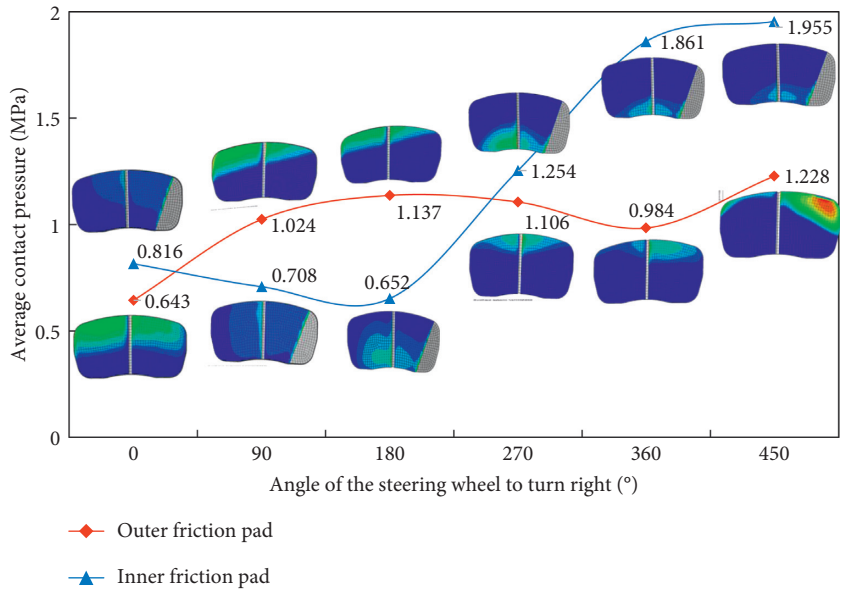

Figure 10: Interface pressure distribution between the pads and disc.

disc [39] is used to describe the deviation of the contact pressure from the reference surface in the whole area. We define the average contact pressure as the reference surface as follows:

$$S_q = \sqrt{\frac{1}{S}\sum(P_i - P_{\text{mean}})^2}, \tag{9}$$

where S is the area of the brake pad and P_{mean} is the average contact pressure. The root mean square deviation of the contact pressure shown in Figure 11. Considering the distribution of contact pressure in Figure 10, the root mean square deviation also increases with an increase in the steering wheel angle, implying that the conditions of steer braking influence the likelihood of squealing.

5.2. Cause of the Interface Pressure Distribution between the Pads and Disc. The distribution characteristics of the interface pressure between the pads and disc can affect the tendency of brake squeal. To determine the reason for the different distributions, attention was focused on the deflection of the interface between the pads and disc. In the FE modeling, the displacement values imposed on the connection points of the suspension (i.e., the force and deformation values transferred from the MBD model) are different, owing to different six-dimensional wheel forces. Therefore, the suspension system produces the reactive forces and torques on the wheel center, mainly through the steering tie rod, low control arm, and strut. These forces and torques are then transmitted to the brake system, which affects the contact state of the pads and disc; here, we consider the steering knuckle for specific analysis.

Figure 12(a) shows that the deflection of the x- and z-axes affects the distribution of the interface pressure. According to the assembly relationship, the disc is connected to the knuckle from the inner flange to the ball to the outer flange, and the pads are connected to the knuckle from the

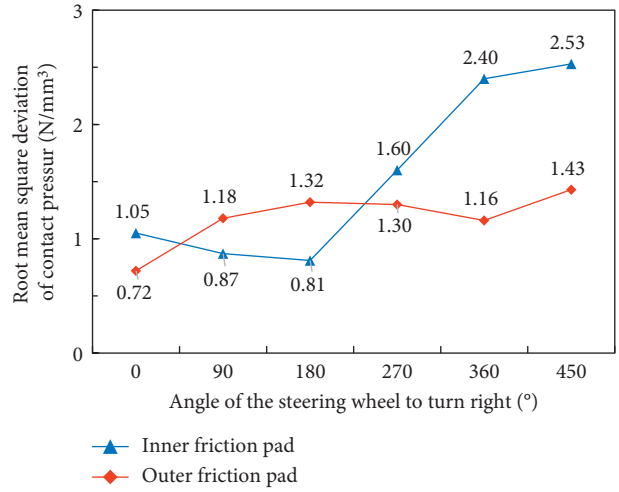

Figure 11: Root mean square deviation of contact pressure.

caliper to the bracket. It is difficult to directly measure the deflection of the interface between the pads and disc; therefore, we measured the angle between the axis of the bracket-knuckle (A_1 in Figure 12(b)) and the axis of the outer flange-knuckle (A2 and A3 in Figure 12(b)). Considering the A_1-axis as a reference axis, the deflection of the A_2-axis around the x-axis and z-axis of the A_1-axis are defined as a_{x1} and a_{z1}, respectively, and the deflection of the A_3-axis around the x-axis and z-axis of the A_1-axis are defined as a_{x2} and a_{z2}, respectively. When a_{x1} and a_{x2} are greater than zero, the contact area of the outer pad tends to move in the z-direction. When a_{z1} and a_{z2} are greater than zero, the contact area of the outer pad tends to move in the $+x$ direction.

Figure 13 shows that the deflection angles are approximately zero during straight-line braking, and the contact pressure between the pads and disc is evenly distributed. With an increase in the steering wheel angle,

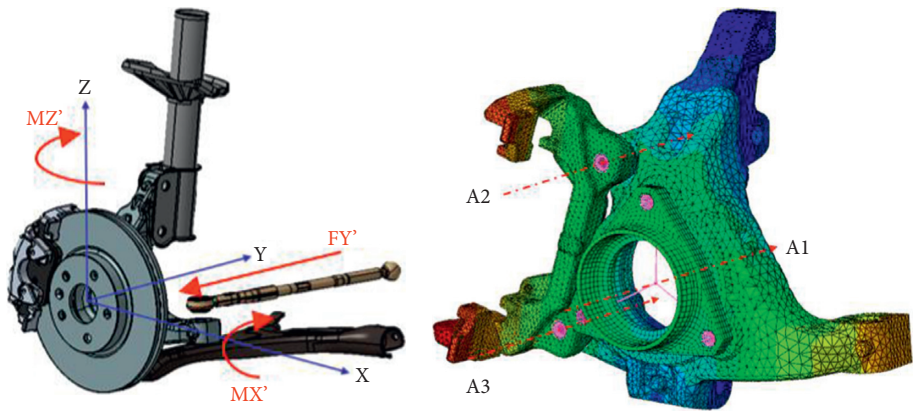

Figure 12: Influence of force and deformation of suspension on interface pressure distribution between the pads and disc. (a) Forces of the suspension system on the wheel center. (b) Deflection axis on knuckle.

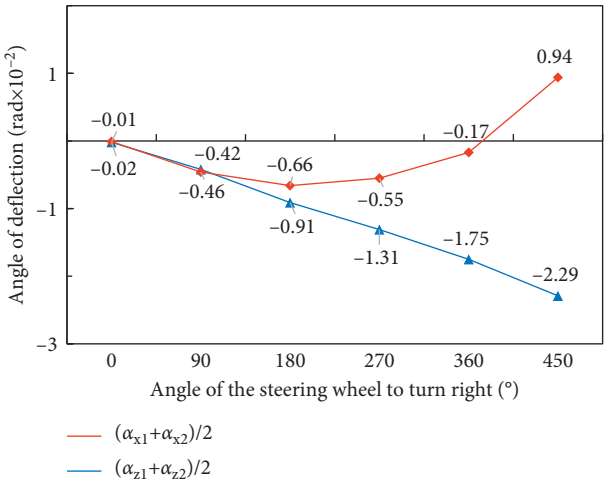

Figure 13: Deflection angles under different steering wheel angles.

the deflection angle around the x-axis first decreases and then increases, and it is less than zero under the conditions of turn right for 1 turn braking and greater than zero under the conditions of turn right for $^4/_5$ turn braking. The deflection angle around the z-axis continues to decrease. In combination with Figure 9, we find that the contact area of the outer pad moves from the upper left to the upper right corner, which is consistent with the variation trend of the deflection angle. The inner pad is directly affected by the pressure of the piston, and the action position is in the middle; thus, it is less affected by the deflection around the x-axis but more affected by the deflection around the z-axis, resulting in the contact area of the inner pad moving towards the lower middle part. In summary, under conditions of steer braking, the stress and deformation of the suspension system cause the axis of the bracket-knuckle to deflect the axis of the outer flange-knuckle, resulting in an uneven distribution of contact pressure between the pads and disc relative to the conditions of straight-line braking; therefore, steer braking is more prone to brake squeal.

6. Conclusion

In this study, a hybrid model was developed for predicting the steering brake squeal propensity, and the mechanism of steering brake squeal was explored. The research established three clearly defined "stages" for steering brake squeal: Stage 1 consists of a road test of steering brake squeal based on a faulty vehicle and extracting the sound, vibration, and other characteristics when squeal occurs. Stage 2 establishes a hybrid modal, including the rigid-flexible coupling and the FED of the front suspension, which is the transferred values of each suspension connection point between the MBD model and FEM. Stage 3 further explores the mechanism of steering brake squeal, and this conclusion can aid the selection of suspension types. The main conclusions of this study are as follows:

(1) In the process of establishing the hybrid model, special attention should be paid to the connection relationship between various parts, and key assumptions should be made according to the actual assembly relationship. To accurately transfer the displacement values between the hybrid models, the mesh information of the chassis corner should be consistent with the suspension components; in particular, the displacement values of each suspension connection point should be used as the transmission medium.

(2) Through the CEA, which is conventionally used for brake squeal propensity prediction, some complex characteristic frequencies appear within 4000 Hz, which are close to the experimental values, indicating that the hybrid model based on MBD and FE methods can accurately predict the steering brake squeal propensity.

(3) Owing to different six-dimensional wheel forces, the displacement values imposed on the connection points are different, and the values lead to an evident deformation of the brake components. As the caliper is indirectly connected to the knuckle, the restraint

condition of the caliper changes, resulting in an uneven distribution of contact pressure between the pads and disc, and is prone to brake squeal. Therefore, it can be considered that the vehicle generates lateral force due to the steering, resulting in the transfer of the sprung mass; the transfer of the sprung mass and the change in tire lateral force leads to different forces and deformations of the suspension system, which change the contact and restraint conditions between the pads and disc, eventually leading to steering brake squeal.

The suggestions for further possible improvements of predicting steering brake squeal propensity can be summarized as follows. Thermomechanical aspect and pad wear need to be considered in the modeling and their effects investigated. Moreover, the factors influencing the steering brake squeal, for example, the structure of brake pads, material properties of parts, and stiffness of connecting bushing, aimed at finding a way to attenuate unstable vibration and brake squeal, should be analyzed. Finally, sample piece production and test verification should be conducted to further examine the solution of the steering braking squeal.

Nomenclature

MBD: Multibody dynamics
FEM: Finite element model
CEA: Complex eigenvalue analysis
EHPS: Electronic hydrostatic power steering
$[M]$, $[C]$, $[K]$, $[K_f]$: Mass matrix, damping matrix, stiffness matrix, and friction stiffness matrix of the pads-on-disc system, respectively
$\{X\}$, $\{\dot{X}\}$, $\{\ddot{X}\}$: Displacement of discrete nodes and their first and second derivatives, respectively
$F_{r,\ w}$, $F_{l,\ w}$: Right and left vertical tire forces, respectively
LTR: Load transfer ratio
ϕ: Roll angle of the vehicle
m, m_1, m_2: Entire vehicle mass, unsprung mass, and sprung mass, respectively
h, h_1, h_{rc}: Roll radius, centroid height of unsprung mass, and ground clearance of roll center, respectively
a_{m2}: Lateral acceleration of the sprung mass
T, Q, Ω: Energy of the system, generalized force vector, and constraint equation, respectively
q, p: Generalized coordinate column vector and Laplace multiplier vector of complete constraints, respectively
μ: Laplace multiplier vector of noncomplete constraints
M_f, K_f, D_f: Mass matrix, stiffness matrix, and damping matrix of the flexible body, respectively
ξ, $\dot{\xi}$, $\ddot{\xi}$: Generalized coordinate and its first, second derivatives, respectively
λ: Lagrange multiplier of the constraint equation
a_k, b_k: Vector of the complex mode and the response, respectively
MAC (a, b): Correlation degree between the ath mode and the bth mode
S_q: Root mean square deviation
S: The area of the brake pad
P_{mean}: The average contact pressure
a_{x1}, a_{z1}: The deflection of A_2-axis around x-axis and z-axis of A_1-axis, respectively
a_{z1}, a_{z2}: The deflection of A_3-axis around the x-axis and z-axis of A_1-axis, respectively.

Data Availability

The data used to support the findings of this study are available from the corresponding author upon request.

Conflicts of Interest

The authors declare that there are no conflicts of interest regarding the publication of this study.

Acknowledgments

This work was supported by National Natural Science Foundation of China (no. 52072270), National Natural Science Foundation of China (no. 51575395), and Shanghai Sailing Program (no. 21YF1449000).

References

[1] C. Cantoni, R. Cesarini, G. Mastinu, G. Rocca, and R. Sicigliano, "Brake comfort - a review," *Vehicle System Dynamics*, vol. 47, no. 8, pp. 901–947, 2009.

[2] N. M. Kinkaid, O. M. O'Reilly, and P. Papadopoulos, "Automotive disc brake squeal," *Journal of Sound and Vibration*, vol. 267, no. 1, pp. 105–166, 2003.

[3] O. Doi, F. Kumamoto, and H. Baba, "A Study on Relationship between Pad Restraint Condition and Brake Squeal Generation," in *Proceedings of the 24th Annual Brake Colloquium and Exhibition Grapevine*, SAE, Grapevine, TX, USA, October 2006.

[4] Z. Lijun, D. Kun, M. Dejian, and Y. Zhuoping, "Time-varying characteristics of frictional squeal in pin-on-disc system: generation mechanism and key impact factors," *Journal of Mechanical Engineering*, vol. 49, no. 14, pp. 99–105, 2013.

[5] O. Giannini, A. Akay, and F. Massi, "Experimental analysis of brake squeal noise on a laboratory brake setup," *Journal of Sound and Vibration*, vol. 292, no. 1-2, pp. 1–20, 2006.

[6] N. Singla, J. Brunel, A. Mège-Revil, H. Kasem, and Y. Desplanques, "Experiment to investigate the relationship between the third-body layer and the occurrence of squeals in dry sliding contact," *Tribology Letters*, vol. 68, no. 1, pp. 234–244, 2020.

[7] S. Oberst and J. C. S. Lai, "A statistical approach to estimate the Lyapunov spectrum in disc brake squeal," *Journal of Sound and Vibration*, vol. 334, pp. 120–135, 2015.

[8] C. Chilbule and D. Weiss, "Analysis of Changes in Disc-Brake Squeal Characteristic Due to Regenerative Braking Simulation on Brake-Inertia-Dynamometer," in *Proceedings of the ThirtySeventh Annual Brake Colloquium and Exhibition*, SAE, Orlando, FL, USA, September 2019.

[9] SAE, *Standard J2521-2013 Disc and Drum Brake Dynamometer Squeal Noise Test procedure*, Brake NVH Standards Committee, New Orleans, LA, USA, 2013.

[10] T. Yokoyama, T. Matsushima, N. Matsui, and R. Misumi, "A Study of Reduction for Brake Squeal in Disc In-Plane Mode," in *Proceedings of the Thirtyth Annual Brake Colloquium and Exhibition*, SAE, New Orleans, LA, USA, September 2012.

[11] C. Kim, Y. Kwon, and D. Kim, "Analysis of low-frequency squeal in automotive disc brake by optimizing groove and caliper shapes," *International Journal of Precision Engineering and Manufacturing*, vol. 19, no. 4, pp. 505–512, 2018.

[12] R. Singh, A. A. Sheikh, and M. J. Mitchell, "Viscoelastic damping to control disc brake squeal," *Sound and Vibration*, vol. 32, no. 10, pp. 18–22, 1998.

[13] F. Chen, "Automotive disk brake squeal: an overview," *International Journal of Vehicle Design*, vol. 51, no. 1-2, pp. 39–51, 2009.

[14] K. Shin, M. J. Brennan, Y.-G. Joe, and J. E. Oh, "Simple models to investigate the effect of velocity dependent friction on the disc brake squeal noise," *International Journal of Automotive Technology*, vol. 5, no. 1, pp. 61–67, 2004.

[15] J. Kang and C. M. Krousgrill, "The onset of friction-induced vibration and spragging," *Journal of Sound and Vibration*, vol. 329, no. 17, pp. 3537–3549, 2010.

[16] N. Hoffmann, M. Fischer, R. Allgaier, and L. Gaul, "A minimal model for studying properties of the mode-coupling type instability in friction induced oscillations," *Mechanics Research Communications*, vol. 29, no. 4, pp. 197–205, 2002.

[17] F. Chen, R. L. Quaglia, and C. A. Tan, "On Automotive Disc Brake Squeal Part I: Mechanisms and Causes," in *Proceedings of the TwentyFirst Annual Brake Colloquium and Exhibition*, SAE, New Orleans, LA, USA, October 2003.

[18] N. Hinrichs, M. Oestreich, and K. Popp, "Dynamics of oscillators with impact and friction," *Chaos, Solitons & Fractals*, vol. 8, no. 4, pp. 535–558, 1997.

[19] H. A. Sherif, "Effect of contact stiffness on the establishment of self-excited vibrations," *Wear*, vol. 141, no. 2, pp. 227–234, 1991.

[20] L. Nechak, S. Berger, and E. Aubry, "Non-intrusive generalized polynomial chaos for the robust stability analysis of uncertain nonlinear dynamic friction systems," *Journal of Sound and Vibration*, vol. 332, no. 5, pp. 1204–1215, 2013.

[21] A. Belhocine and W. Z. W. Omar, "Three-dimensional finite element modeling and analysis of the mechanical behavior of dry contact slipping between the disc and the brake pads," *International Journal of Advanced Manufacturing Technology*, vol. 88, no. 1-4, pp. 1035–1051, 2017.

[22] A. Belhocine, "FE prediction of thermal performance and stresses in an automotive disc brake system," *International Journal of Advanced Manufacturing Technology*, vol. 89, no. 9-12, pp. 3563–3578, 2017.

[23] A. Belhocine and N. M. Ghazaly, "Effects of material properties on generation of brake squeal noise using finite element method," *Latin American Journal of Solids and Structures*, vol. 12, no. 8, pp. 1432–1447, 2015.

[24] A. Belhocine and O. I. Abdullah, "Thermomechanical model for the analysis of disc brake using the finite element method in frictional contact," *Multiscale Science and Engineering*, vol. 2, no. 1, pp. 27–41, 2020.

[25] A. Belhocine, D. Shinde, and R. Patil, "Thermo-mechanical coupled analysis based design of ventilated brake disc using genetic algorithm and particle swarm optimization," *JMST Advances*, vol. 3, no. 3, pp. 41–54, 2021.

[26] D. Kun, Z. Lijun, M. Dejian, and Y. Zhehao, "Improvement of prediction accuracy of brake squeal with complex modal FE mode," *Automotive Engineering*, vol. 35, no. 10, pp. 908–914, 2013.

[27] Z. Zhang, W. Li, and D. Meng, "Propagation regularity of disc brake squeal uncertainty from friction coefficient," *Tongji Daxue Xuebao/Journal of Tongji University*, vol. 45, pp. 167–174, 2017.

[28] J.-J. Sinou, "Transient non-linear dynamic analysis of automotive disc brake squeal - on the need to consider both stability and non-linear analysis," *Mechanics Research Communications*, vol. 37, no. 1, pp. 96–105, 2010.

[29] K. Shang, X. Liu, and E. Moureh-Ledig, "Squeal simulation and analysis of brake system with pressure and speed dependent friction model and exerting process of pressure," *Journal of Vibroengineering*, vol. 19, no. 3, pp. 2090–2105, 2017.

[30] O. Stump, R. Nunes, K. Haesler, and W. Seemann, "Linear and non-linear stability analysis of a fixed caliper brake during forward and backward driving," *Journal of Vibration and Acoustics*, vol. 89, no. 95, pp. 69–74, 2018.

[31] R. Rajamani and D. N. Piyabongkarn, "New paradigms for the integration of yaw stability and rollover prevention functions in vehicle stability control," *IEEE Transactions on Intelligent Transportation Systems*, vol. 14, no. 1, pp. 249–261, 2013.

[32] S. Ke, *Theoretical Research on Vehicle Rollover Mechanism and Active Steering Rollover Prevention control*, Hefei University of Technology, Hefei, China, 2019.

[33] J. Otto, G. Ostermeyer, and S. Rhee, *On the Wear Dependence of Low-Frequency and High-Frequency Brake Squeal*, SAE International, Palm Desert, CA, USA, 2018.

[34] M. T. B. A. Dos, J. C. Horta Gutiérrez, C. J. Ferreto, F. D. Silva, and L. V. Donadon, *Influence of pads and brake disc wear on brake squeal noise*, SAE International, Caxias do Sul, Brazil, 2020.

[35] Z. Yibing, *Influence Mechanism of Suspension Comprehensive Mechanical Characteristics on Brake groan*, Tongji University, Shanghai, China, 2016.

[36] L. Zhang, X. Zhang, and D. Meng, "Experimental study on transient characteristics and key factors of vehicle Brake Groan," *Journal of Mechanical Engineering*, vol. 54, no. 24, pp. 118–128, 2018.

[37] H. Yang, Y. Lin, C. Hsiao, and J. Y. Liu, "Evaluating residual compressive strength of concrete at elevated temperatures using ultrasonic pulse velocity," *Fire Safety Journal*, vol. 44, no. 1, pp. 121–130, 2009.

[38] G. Dihua and J. Dongying, *A Study on Disc Brake Squeal Using Finite Element methods*, SAE Technical Paper, Warrendale, PA, USA, 1998.

[39] W. Song, *Evaluation of Three-Dimensional Surface Topography and its application*, Nanjing University of Aeronautics and Astronautics the Graduate School, Nanjing, China, 2007.